Weather conditions leading to deadly wildfires in Türkiye, Cyprus and Greece made 10 times more likely due to climate change

Authors

Theodore Keeping, *Centre for Environmental Policy, Imperial College, London, UK*
Claire Bergin*, ICARUS Climate Research Centre, Maynooth University, Maynooth, Ireland*
Izidine Pinto, *Royal Netherlands Meteorological Institute (KNMI), De Bilt, The Netherlands*
Bikem Ekberzade, *Istanbul Technical University, Eurasia Institute of Earth Sciences, Istanbul, Türkiye*
Apostolos Voulgarakis, *Technical University of Crete, Greece; Leverhulme Centre for Wildfires, Environment and Society, Imperial College London, London, UK*
Manolis Grillakis, *Technical University of Crete, Greece; Leverhulme Centre for Wildfires, Environment and Society, Imperial College London, London, UK*
Georgios Papavasileiou, *National Observatory of Athens, Institute for Environmental Research and Sustainable Development, Greece*
Gavriil Xanthopoulos, *Hellenic Agricultural Organization "DIMITRA", Institute of Mediterranean Forest Ecosystems (ret.)*
Kostas Lagouvardos, *National Observatory of Athens, Institute for Environmental Research and Sustainable Development, Greece*
Theodore Giannaros, *National Observatory of Athens, Institute for Environmental Research and Sustainable Development, Greece*
Ismail Yucel, *Middle East Technical University, Civil Engineering Department, Water Resources Division, Ankara, Türkiye*
Hatice Atalay, *Izmir Katip Celebi University, Engineering and Architecture Faculty, Geomatics Engineering Dept., 35620, Izmir, Türkiye*
Clair Barnes, *Centre for Environmental Policy, Imperial College, London, UK*
Maja Vahlberg, *Red Cross Red Crescent Climate Centre, The Hague, the Netherlands; Swedish Red Cross, Stockholm, Sweden (based in Ubmeje/Umeå, Sweden)*
Aynur Kadihasanoglu*, Red Cross Red Crescent Climate Centre, The Hague, the Netherlands*
Roop Singh*, Red Cross Red Crescent Climate Centre, The Hague, the Netherlands (based in New Jersey, USA)*
Dilan Çağla Tunç*, Turkish Red Crescent, Ankara, Türkiye*
Friederike Otto, *Centre for Environmental Policy, Imperial College, London, UK*

Review authors

Sjoukje Philip, *Royal Netherlands Meteorological Institute (KNMI), De Bilt, The Netherlands*
Mariam Zachariah , *Centre for Environmental Policy, Imperial College, London, UK*
Dora Vrkić, *Grantham Institute - Climate Change and the Environment, Imperial College London, London, UK*
Pelin Koç, *IFRC Türkiye Delegation, Ankara, Türkiye*
Selahattin Horozaloğlu, *Turkish Red Crescent, Ankara, Türkiye*
Muhammet Ali Erduran, *Turkish Red Crescent, Ankara, Türkiye*
İlker Girit, *Turkish Red Crescent, Ankara, Türkiye*
Evgenia Gkogkou, *Hellenic Red Cross, Athens, Greece*
Paula Haro, *IFRC Regional Office for Europe, Budapest, Hungary*
Emmanuel Raju, *Copenhagen Centre for Disaster Research, University of Copenhagen*

Main findings

- Türkiye, Greece and Cyprus are exposed to different types of wildfire events and impacts. While Türkiye and Greece face similar challenges with large-scale fires that can span multiple provinces, large summer tourist populations and fire-conducive environments, the wildland urban interface (WUI) in Turkiye is mainly in coastal tourist areas and inland forest villages, whereas in Greece the risk is particularly high in dense island settlements and in the Attica suburbs presenting different firefighting and evacuation challenges. Cyprus faces concentrated risks due to its small size and reliance on aerial support for large fires.
- Empirical weather data suggest that, in today's climate which is warmer by 1.3°C relative to preindustrial times, the extreme conditions that drove the recent wildfires are expected to occur approximately once every 20 years. Compared to a 1.3°C cooler climate this is an increase in likelihood of about a factor of 5 and an increase in the intensity of the DSR of about 14%. Meaning the event as characterised by the DSR over the region outlined above would only be expected to occur once per 100 years without climate change.
- Looking at the observations for VPD7x gives similar results: The event in today's climate is about a 1 in 10 year event, whereas in a 1.3°C cooler climate, it would be expected to occur once in every 100 years. The intensity has increased by about 16%.
- To determine the role of climate change in this observed trend we combine the observation-based estimates with climate models. For both indices the models on average show a stronger increase in likelihood and intensity than observed. This leads to an overall increase in VPD7x of a factor of about 13 and an increase in intensity of about 18% attributable to human-induced climate change. For DSR the overarching increase in likelihood due to climate change is a factor 10 and an increase in intensity of also about 22%.
- With a further 1.3°C of global warming, causing global temperatures to reach 2.6°C, which is expected this century under current policies, the projected VPD7x conditions are 18% more intense and about six times more likely to occur, compared to now. The DSR is projected to become another 25% more intense and another nine times more likely.
- In the winter months leading up to the wildfires, in general, it was dry in Greece and wet in Türkiye. However, across the last number of years there is an overall drying trend in both regions, with this trend stronger in Türkiye. Looking at overall rainfall observation totals during the pre-fire season, October to April, we observe these totals to have decreased by around 14%. It should be noted that the timing and duration of pre-season rainfall can act as an early indicator of potential wildfire risk, as well as the total rainfall over the period. Rainfall volume and timing can strongly affect the pre-season growth of some vegetation types, such as grasses, the amount of which can in turn affect the susceptibility to extreme wildfire.
- This finding is corroborated by assessing the drought code, which is part of the Fire Weather Index used to calculate DSR. The drought code at the time of and preceding the fires showed that this was, on average, one of the driest years ever recorded.
- To analyse potential changes in weather patterns, in particular the northerly winds that made the fires spread quickly, we characterise the observed weather pattern based on the Z500 geopotential height and assess similar patterns, so called analogues over two time periods: 1951–1980 and 1994-2023. The 1951-1980 pattern shows weaker high-pressure systems and a less intense northward ridge, with a more noticeable difference between north and south. In

contrast, the 1994–2023 pattern looks much more like what we saw in 2025 — with higher pressure (Z500 values) and a stronger ridge stretching further north. This change suggests that these types of high-pressure systems have become more intense, leading to more intense heat and stronger northerly winds.

- The simultaneous occurrence of highly impactful wildfires across Europe highlights the current strain on firefighting resources in the current climate with 1.3°C of warming. This year, the EU Civil Protection Mechanism, responsible for coordinating aid and support during emergencies, has been activated 17 times in response to wildfires, including in Greece, Albania, Bulgaria, and Spain over seven days. With further warming, more extreme, concurrent fire-weather will continue to challenge firefighting resources and push the limits of adaptation in some places.
- Türkiye, Greece, and Cyprus have all strengthened wildfire management and response in recent years through new technologies, expanded firefighting forces, and stricter legal frameworks. Türkiye has invested in aerial fleets, AI detection, and large volunteer networks; Greece has scaled up drones and specialized units; Cyprus has developed satellite-based detection. As climate change increases risks, adaptation efforts can be strengthened by further educating the public about wildfire risks and fire safety behaviors, increasing investment in proactive wildfire mitigation and management, and integrating Indigenous, traditional, and contemporary fire management practices into policy.

1 Introduction

In July 2025, Türkiye, and Cyprus faced one of the most severe wildfire crises in recent memory, as extreme heat, prolonged drought, and strong winds created conditions that drove devastating blazes across the Eastern Mediterranean. A record-breaking heatwave, with temperatures soaring above 45°C, intensified fire conditions, forcing mass evacuations, killing and injuring firefighters, and leaving vast swathes of land scorched (IFRC, 2025).

In Greece, wildfires swept through the Peloponnese, Attica, Crete, Evia, and Kythera, triggering the evacuation of at least 32,000 people, including 5,000 tourists on Crete (IFRC, 2025; Le Monde, 2025; Argophilia, 2025). Entire communities were uprooted as tens of thousands of acres of farmland, homes, and tourist resorts were consumed by flames—Kythera alone suffered widespread devastation (Giannopoulos, 2025). At least 13 firefighters were injured while responding to the crisis, and the destruction significantly disrupted both local livelihoods and the vital tourism sector. The Feneos, Corinth wildfire burned 1,579 ha, including extensive Kefalonian Fir forests and two Natura 2000 areas, making it the season's most severe ecological loss. Although winds were weak, the combination of prolonged drought, near-surface atmospheric aridity, and a favorable vertical structure of the atmosphere increased fuel flammability, driving intense burn and fire-atmosphere interactions. The fire evolved into a plume-dominated event, marked by pyroconvection, pyrocloud formation, plume rotation, strong updrafts, long-range spotting, and chaotic spread (Giannaros et al., 2025).

Cyprus experienced its worst wildfires in decades. Intense heat, wind, and drought conditions sparked massive fires north of Limassol, leading to the tragic deaths of two people fleeing the village of

Monagri. Approximately 125 square kilometers—about 1% of the island—were destroyed, forcing evacuations from 14 villages (Euronews, 2025; Reuters, 2025). Over 70 homes were damaged, with farms, vineyards, and power infrastructure also affected. More than 250 firefighters, supported by international aid, worked under extreme conditions to contain the flames (Al Jazeera, 2025). Environmental economists estimate that the indirect ecological damage, such as loss of ecosystem services like erosion protection and biodiversity, could range between €1,000 and €2,000 per hectare. Applying this to an affected area of ~125 km² yields an estimated environmental cost of €10–20 million (Cyprus Economic Society, 2025).

Meanwhile, Türkiye endured one of its most destructive wildfire seasons on record, losing more forest area in a single month than any other Mediterranean country in 2025. According to the General Directorate of Forestry, 612 forest fires erupted in June alone—rising to 624 by early July (Anadolu Agency 2025). Hot, dry summers in Türkiye's Mediterranean and Aegean regions have become increasingly prolonged and intense due to accelerating climate change, increasing the frequency, scale and severity of wildfire outbreaks. The country's fire-adapted *Pinus brutia* forests and maquis understory re-establish through cyclical wildfires. However, as meteorological conditions become extreme, ameliorating the spread of wildfires to adjacent forest belts in different altitudes and in complex terrain, long-term ecological impacts from changes in vegetation composition of the region's forests becomes a major concern. Taxa, such as *Pinus nigra*, *Cedrus libani* and *Abies* subspecies that cannot survive high intensity crown fires, and thus are at great risk from potential changes in the fire regime, become vulnerable, and any potential and permanent loss in forest cover translates into a major disruption of ecosystem services as well as now face long-term ecological impacts, including degraded soil fertility and reduced agricultural potential (Iban, 2022).

Western and northwestern provinces of Türkiye, such as Izmir, Bursa, Manisa, Bilecik, Çanakkale, Karabük, and Hatay, were among the hardest hit. In Izmir, fires ravaged entire towns in Seferihisar and Çeşme, prompting the evacuation of around 50,000 residents and causing severe property losses. The Seferihisar (Orhanlı) fire in Izmir demonstrated exceptional wind-driven behavior, spreading nearly 12.8 km in under three hours under winds of 50 km/h and wind gusts up to 80 km/h, with rapid surface and crown fire runs accompanied by extensive spotting (Coskuner and Papavasileiou, 2025) Strong coastal winds in Çeşme, a major windsurfing destination, further hampered firefighting efforts and damaged local businesses. In Manisa's Akhisar district, a fire that began from a beekeeper's attempt to smoke bees quickly escalated into a major blaze (Bianet, 2025). During the second wildfire that started in Çanakkale, in close proximity to the Dardanelles Strait in August, spread quickly due to high surface wind speeds, urging authorities to evacuate the campuses of Çanakkale 18 Mart University (Reuters, 2025)

Nationwide, more than 50,000 people were evacuated between late June and July as fires spread rapidly from rural areas to urban fringes. In total, at least 17 lives were lost, including 10 firefighters and rescue workers operating in Eskişehir in northwestern Türkiye, who died as extreme winds closed in on their exit route (Anadolu Agency 2025, Echo Flash, 2025, Al Jazeera, 2025). The wildfires in Izmir alone caused three deaths, left hundreds affected by smoke inhalation, and damaged over 200 homes and businesses. Major highways like the Bursa-Ankara route were temporarily closed, highlighting the growing threat of wildfires to both rural communities and major population centers (Bianet, 2025, Reuters, 2025).

In terms of meteorology, the *Etesians* (a seasonal pattern of strong, dry northerly winds) primarily affect the Aegean region, including the eastern mainland and surrounding islands. Typically dominant during July and August, recent patterns indicate their increasing frequency as early as June. While the Etesians can lead to a moderate decrease in ambient temperatures, their high velocity and persistent nature can exacerbate wildfire conditions. These winds known to fan existing fires can intensify active fires, hinder suppression efforts, and accelerate the spread of flames across both insular and mainland terrains. As an example, the fire in southern Chania-Crete (Paliochora-Azogire region) in late July 2025 was fueled by Etesian winds that were intensified by the Foehn effect. As the Etesians blew from the north and crossed the high Lefka Ori mountains at the center of the island, the air lost much of its moisture on the windward side. When it descended toward the south slopes, it became hotter and drier. This warm, dry downslope flow created ideal conditions for the fire to spread quickly. Local weather stations nearby the fire recorded sustained winds to as high as 79km/h and relative humidity of the air to as low as 21%.

From 25 to 26 July, a dominant upper-level ridge was centered over Greece, Türkiye, and the southern Balkans, producing hot and stable surface conditions, accompanied by strong northerly winds across the Aegean and eastern Greece, conditions that fueled multiple wildfires during this period. Extreme heat affected areas marked with dots, indicating temperature anomalies exceeding two standard deviations above the 1991–2020 climatological mean. These months in Türkiye also exhibited a shift from typical seasonal norms. During this period, winds were predominantly from the north, consistent with the local Etesian wind pattern over the Aegean Sea. These north-northerly Etesian winds can become dangerous during extreme heat events. This type of circulation is often linked to the development and spread of major wildfire events in Greece and Türkiye (citation).

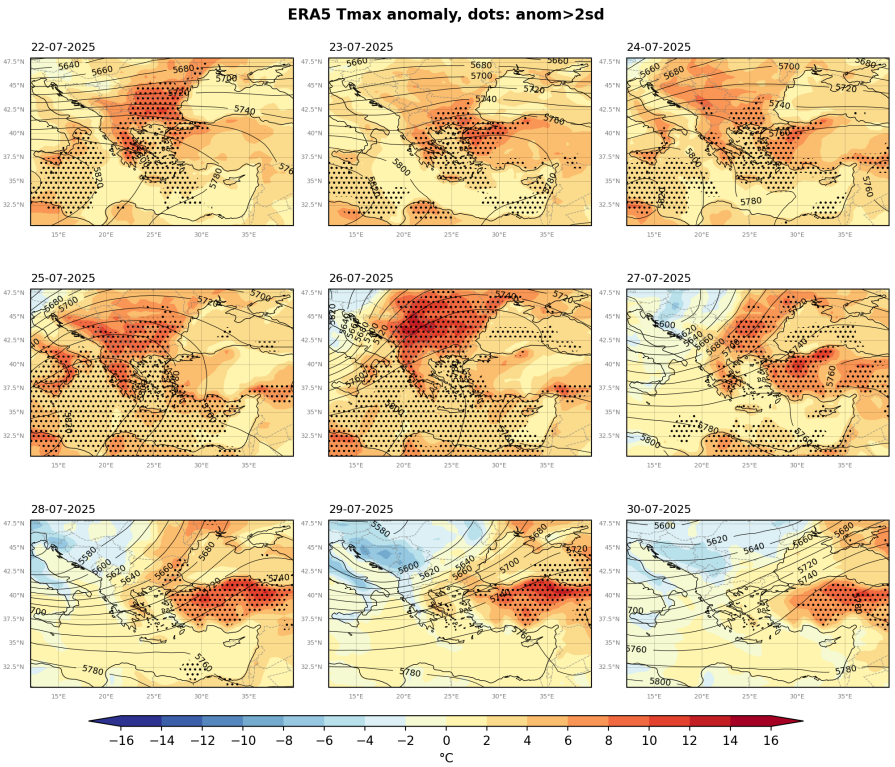

Figure 1.1*: Daily maximum temperatures with pressure levels included to show the dominant windspeed direction (broadly from high to low pressure).*

1.1 Wildfires in Aegean Greece and Türkiye

Several studies on fire weather conditions in the Mediterranean, including Greece and Türkiye, show that fire danger is expected to progressively increase in the future (Malisovas et al., 2023; Xepapadeas et al., 2024; Ekberzade et al., 2025; Turco et al., 2018; Giannaros and Papavasileiou, 2023). Based on century-long historical records in Greece, Koutsias et al., (2013) show that rising air temperatures, especially after the mid-1970s, coincide with increasing fire occurrence, with fire activity to be primarily driven by heatwaves and low precipitation during the fire season. More recently, Papavasileiou and Giannaros (2024) reported significant positive trends in the occurrence of critical fire weather patterns associated with hot, dry, and windy conditions. Rovithakis et al., (2022) show that especially in the high-end climate change scenario with southern and eastern regions of Greece expected to have up to 40 additional days of high fire danger relative to the late 20th century, on average. Crete, the Aegean Islands, the Attica region, as well as parts of Peloponnese are predicted to experience a stronger increase in fire danger. In addition, Rovithakis et al. (2025) show that hotter and drier conditions will drive future increases in burnt area across Greece, especially in the southern regions, where flammable and heat-resistant needleleaf species exist.

There are very few studies explicitly looking at the role of climate change in fire weather over Türkiye. However, an individual study looking at FWI along the Türkish coast found a decreasing trend (Ertogrul et al., 2021), which is in contrast to the other studies referenced above and more general assessments of climate change indicators, such as high temperatures, increasing drought risk and decreasing precipitation, all of which are found to be significant in the Eastern Mediterranean region and summarised e.g. in the IPCC (Seneviratne et al., 2021, Bağçaci et al., 2024).

1.2 Event Definition

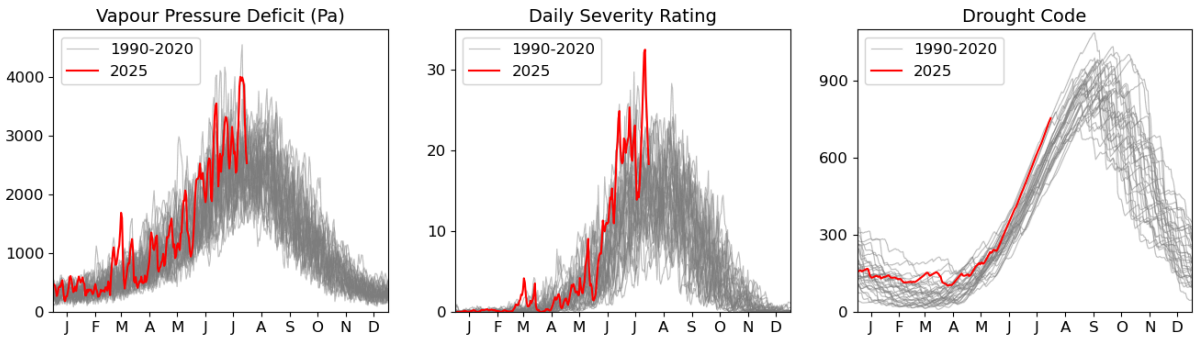

Figure 1.2: *The annual cycle in VPD (left), DSR (daily severity rating of the Canadian FWI - centre) and drought code (DC - right) for 2025 compared to the 1990-2020 annual cycles.*

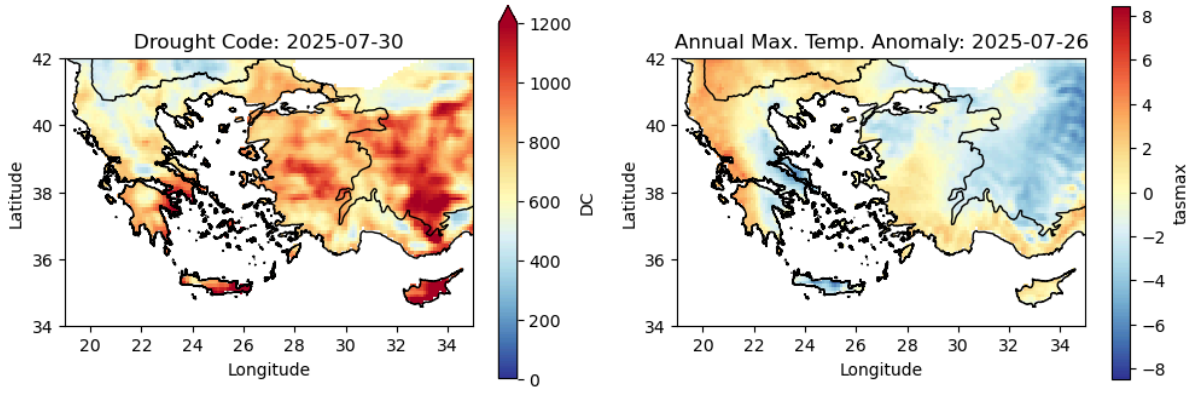

Figure 1.3: *Left, the drought code on the 30th July, 2025. Right, the maximum daily temperature on 26th July, 2025, compared to the average annual maximum temperature in the 1990-2020 period.*

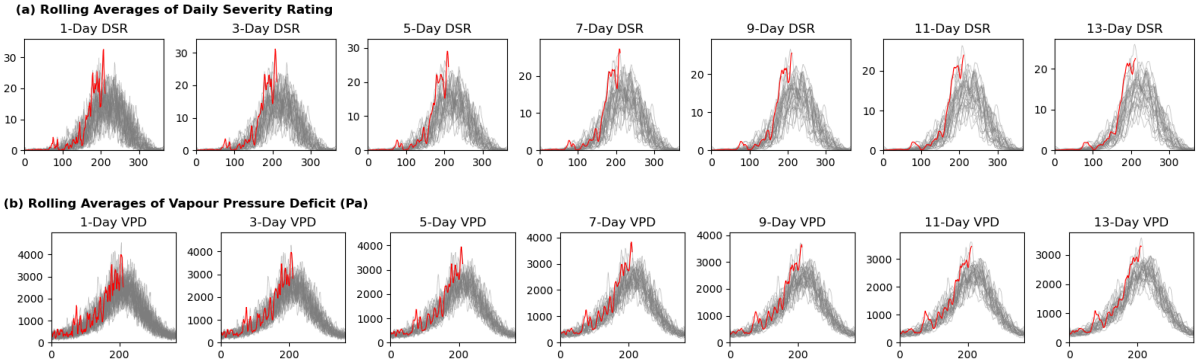

Figure 1.4: *the* ***(a)*** *DSR and* ***(b)*** *VPD at different rolling-window daily means.*

As wildfire is a product of atmospheric and vegetation conditions, a relatively ecologically homogeneous region was chosen for this study. The Mediterranean biogeographic region (EEA, 2025) is characterised by hot summers and semi-arid vegetation, especially including evergreen trees and shrubs, as well as a large number of aromatics, and is highly prone to wildfire. The precise region considered was the region within the Mediterranean Biogeographic Region (defined by the EEA) confined by 19°-35°E and 33°-42°N. All indices were averaged over this region.

Very hot, dry conditions in conjunction with the Etesian winds gave rise to the extreme wildfire behaviour seen in the Mediterranean regions of Greece, Türkiye and Cyprus considered in this study. We characterise this event using the following event definitions:

- The annual maximum of the 3-day Daily Severity Rating (DSR3x). This is a composite index for long term trends in fuel moisture, hot and dry weather and wind, widely adopted in Mediterranean Europe. The Daily Severity Rating is a rescaling of the Canadian Fire Weather Index (FWI) intended for accumulation over multi-day periods and ecologically homogeneous regions.
- The annual maximum of the 7-day vapour pressure deficit (VPD7x). This accounts for the effect of heat on extremely-dry wildfire-prone fuel conditions, with VPD characterising the atmospheric drying demand due to heat and humidity.
- Seasonal precipitation levels were investigated in observations only as part of an investigation to ascertain if the area in question was particularly dry or flush with vegetation preceding the

wildfires. Three different land masses were investigated. The first is the whole 'Mediterranean' area defined above. This Mediterranean area is then split along 26°E, roughly corresponding to Greece to the west, and Türkiye and Cyprus to the east. These regions were investigated for the total rainfall during October-April, as rainfall in this period has a strong effect on the extent to which soil moisture stress affects vegetation growth.

- The drought code (DC), a sub-index of the FWI, was also examined. The DC characterises the response of moisture in larger dead wood and the deeper layers of plant litter to long-term dry conditions.

From 25 to 26 July, a dominant upper-level ridge was centered over Greece, Turkey, and the southern Balkans, producing hot and stable surface conditions. During this period, winds were predominantly from the north, consistent with the local Etesian wind pattern over the Aegean Sea. This type of circulation is often linked to the development and spread of major wildfire events in Greece and Turkey (citation). We assess the changing frequency and intensity of analogues to this circulation pattern in the observed record.

In this report, we study the influence of anthropogenic climate change by comparing the likelihood and intensity of similar extremes at present with those in a 1.3°C cooler climate. We also extend this analysis into the future by assessing the influence of a further 1.3°C of global warming from present. This is in line with the latest Emissions Gap Report from the United Nations Environment Programme, which shows that the world is on track for at least 2.6°C temperature rise given currently implemented policies (UNEP, 2024).

2 Data and methods

2.1 Observational data

We first use observational and reanalysis data to estimate the return period of a similar event in the present day and to assess the historical trends with increasing GMST. The datasets used are as follows:

- EOBS humidity and windspeed did not extensively cover study area, so was only used for precipitation attribution.
- ERA5-Land used for VPD and DSR attribution
- ERA5 and EOBS were used for the precipitation attribution.

ERA5 - The European Centre for Medium-Range Weather Forecasts's 5th generation reanalysis product, ERA5, is a gridded dataset that combines historical observations into global estimates using advanced modelling and data assimilation systems (Hersbach et al., 2020). We use VARIABLE data from this product at a resolution of 0.5°×0.5° / 0.25°×0.25°, from the years 1950 to present.

ERA5-Land - This product is a replay of the land component of the ERA5 climate reanalysis (Muñoz-Sabater et al., 2021) produced by the European Centre for Medium-Range Weather Forecasts, with a finer spatial resolution of 0.1° (~9km grid spacing), at hourly time steps from 1950 to 5 days before the current date. The land model used is the tiled ECMWF Scheme for Surface Exchanges over

Land incorporating land surface hydrology (H-TESSEL). We use VARIABLE data from this product at a resolution of 0.5°×0.5° / 0.25°×0.25°, from the years 1950 to present.

E-OBS - This is a gridded land-only observation dataset of Europe, formed from the interpolation of station‑derived meteorological observations (Cornes et al., 2018). We use version 29.0e of this dataset, at spatial resolution 0.25° × 0.25° gridded VARIABLE, from 1920-present.

2.2 Model and experiment descriptions

We use two multi-model ensembles from climate modelling experiments using very different framings (Philip et al., 2020): Sea Surface temperature (SST) driven global circulation high resolution models, coupled global circulation models and regional climate models.

Due to the fact that this is a coastal and island region, high resolution models were required to sufficiently capture the event. The models used were therefore taken from EURO-CORDEX and HighResMIP, and not from the main CMIP6 experiment ensemble.

1. Coordinated Regional Climate Downscaling Experiment (CORDEX)- European Domain (EURO-CORDEX) with 0.11° resolution (EUR-11) (Jacob et al., 2014; Vautard et al., 2021). The ensemble of models used for this study consists of 4 regional climate models each of which are driven by up to 6 GCMs for a total of 13 models. These simulations are composed of historical simulations up to 2005, and extended to the year 2100 using the RCP8.5 scenario.

2. HighResMIP SST-forced model ensemble (Haarsma et al. 2016), the simulations for which span from 1950 to 2050. The SST and sea ice forcings for the period 1950-2014 are obtained from the 0.25° x 0.25° Hadley Centre Global Sea Ice and Sea Surface Temperature dataset that have undergone area-weighted regridding to match the climate model resolution. For the ‘future’ time period (2015-2050), SST/sea-ice data are derived from RCP8.5 (CMIP5) data, and combined with greenhouse gas forcings from SSP5-8.5 (CMIP6) simulations (see Section 3.3 of Haarsma et al. 2016 for further details).

2.3 Statistical methods

Methods for observational and model analysis and for model evaluation and synthesis are used according to the World Weather Attribution Protocol, described in Philip et al., (2020), with supporting details found in van Oldenborgh et al., (2021), Ciavarella et al., (2021), Otto et al., (2024) and here. The key steps, presented in sections 3-6, are: (3) trend estimation from observations; (4) model validation; (5) multi-method multi-model attribution; and (6) synthesis of the attribution statement.

For each time series we estimate the parameters of a statistical model in which the index depends on the GMST. This model is then used to estimate the return period and intensity of the event under study for the 2025 GMST and for a 1.3°C cooler counterfactual climate: this allows us to compare the expected intensity and frequency of similar events now and in the preindustrial past (1850-1900, based on the Global Warming Index), by calculating the probability ratio (PR; the factor-change in the event's probability) and change in intensity of the event

A nonstationary log-normal distribution is used to model both DSR3x and VPD7x. In each case, the distribution of log-transformed DSR3x/VPD7x is assumed to shift linearly with the GMST covariate, while the variance remains constant. The parameters of the statistical model are estimated using maximum likelihood.

3 Observational analysis: return period and trend

3.1 Analysis of Hot, Dry and Windy Annual Maxima

Linear trends in annual 3-day DSR maxima in the ERA5-Land dataset (Fig. 3.1) show an increasing trend over most of the study region, except on the southern coast of Türkiye where there is a decreasing trend. Ertogrul et al. (2021) find a decreasing fire effect over parts of southwestern Türkiye, but do not provide a comprehensive overview of spatial differences in the trend. We confirm that there is indeed a decreasing trend in some parts of Türkiye, but that these are confined to the southern Mediterranean coast of Türkiye - and not the regions of Marmara and the Aegean, which were the most affected by this year's wildfires. There is also a widespread positive trend in annual 7-day VPD maxima, with decreasing trends confined to small subregions of the southern Turkish Mediterranean.

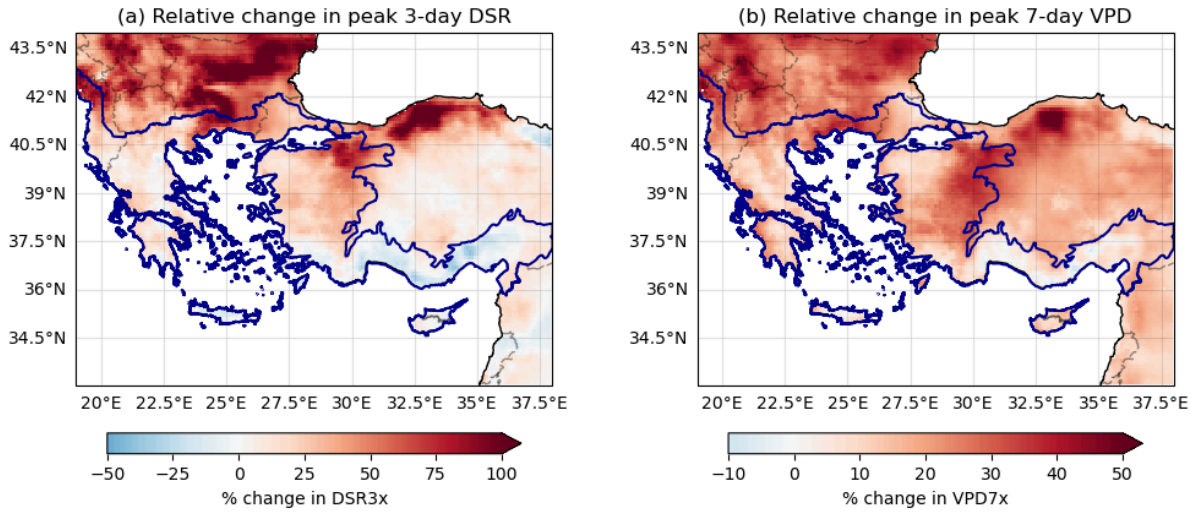

Figure 3.1: *Linear trends at each grid cell in ERA5-Land for* ***(a)*** *DSR3x and* ***(b)*** *VPD7x. The study region is outlined in dark blue.*

Table 3.1 summarises the return periods and event magnitude for the 3-day averaged DSR and 7-day averaged VPD in ERA5-Land. The DSR3x conditions are currently expected to be an approximately 1-in-20 year event and the VPD7x conditions an approximately 1-in-10 year event. The table also describes the probability ratio of those events in pre-industrial and present climates according to the attribution analysis. According to this observational data, the likelihood of DSR3x events of at least this magnitude has increased by about 4.5 times – with a 95% confidence interval from 0.6 to 47. The likelihood of the longer-period VPD7x has increased by about 11 times – with a 95% confidence interval of about a 1.7 to 110 times increase. The intensity of a 3-day DSR event of this year's return period has increased by approximately 14%. The intensity of a 7-day VPD event of the same return

period has increased by 16%. VPD strongly relates to some components of the Canadian fire weather index, such as rapid fine fuel drying in hot and dry conditions, so the shift in DSR will have been significantly contributed to by this shift in VPD - though other factors contributing to DSR (such as wind speeds and drought conditions) will also have had an effect. Both models (Fig. 3.2 and 3.3) were fit using a log-normal distribution, and show good fit to the data (right panels). We did not exclude the early years of the data (the 1950s) from the fits, even though they seem to have higher values, because 1) we do not have the possibility to check whether these values are real or an artefact and 2) the precipitation values (Sect 3.2) show similar behaviour in both ERA5 and E-OBS. ERA5-Land was used for this analysis due to its good performance over the region and high resolution capturing fire weather extremes. EOBS was also assessed however historical relative humidity coverage meant that it could not be used for the region.

Table 3.1: *Estimated return periods of DSR3x and VPD7x over Mediterranean Greece, Türkiye and Cyprus in the ERA5-Land reanalysis dataset.*

Data set	DSR3x				VPD7x			
	Magnitude	Return period (95% C.I.)	Probability ratio PR	Change in intensity ΔI [%]	Magnitude (Pa)	Return period (95% C.I.)	Probability ratio PR	Change in intensity ΔI [%]
ERA5-Land	31.2	18.5 (7.38…98.3)	4.54 (0.572…47.0)	14.4 (-4.18…36.1)	3830	10.4 (4.75…38.5)	10.7 (1.76…110)	15.8 (3.15…30.0)

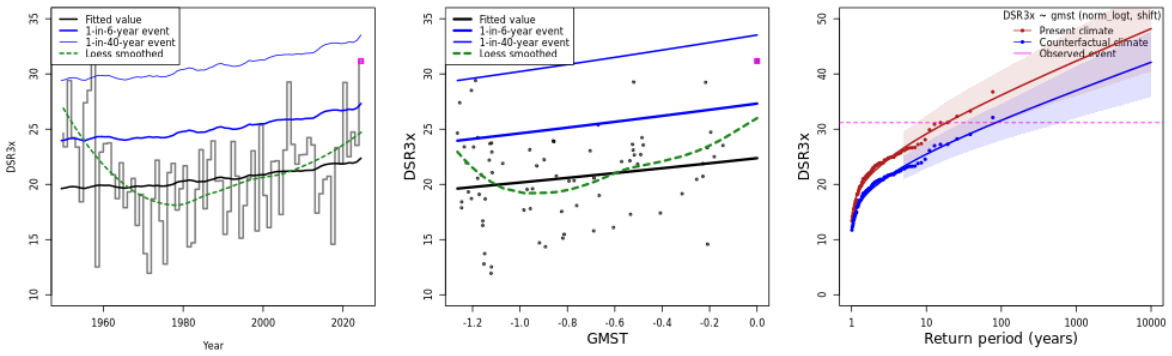

Figure 3.2*: (Left) the trend against time in the annual maximum 3-day DSR. (Centre) the trend against GMST in the annual maximum 3-day DSR. (Right) the log-normal shift of the annual maximum 3-day DSR distribution to GMST, return periods are shown for the 2025 climate (red) and a climate with GMST 1.3ºC cooler (blue). The reanalysis data are shown twice: once shifted up to the current climate and once shifted down to the climate of the pre-industrial era. The markers show the data and the lines show the fits and uncertainty from the bootstrap.*

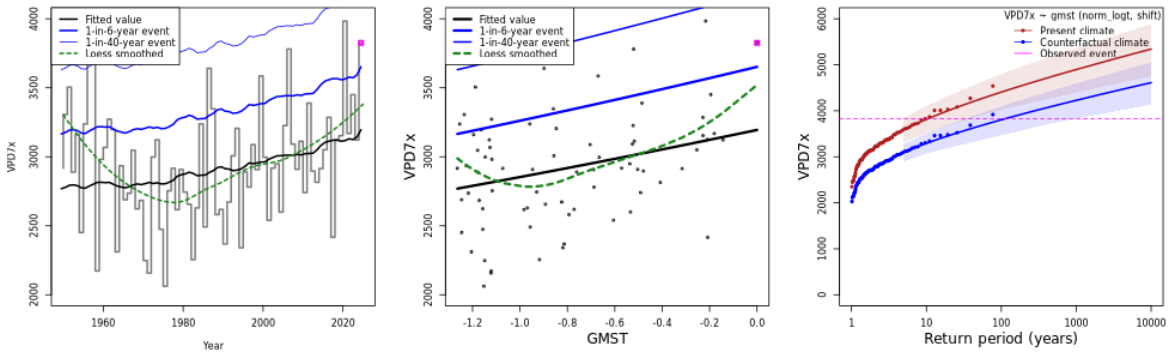

***Figure 3.3**: (Left) the trend against time in the annual maximum 7-day VPD. (Centre) the trend against GMST in the annual maximum 7-day VPD. (Right) the log-normal shift of the annual maximum 7-day VPD distribution to GMST, return periods are shown for the 2025 climate (red) and a climate with GMST 1.3ºC cooler (blue). The reanalysis data are shown twice: once shifted up to the current climate and once shifted down to the climate of the pre-industrial era. The markers show the data and the lines show the fits and uncertainty from the bootstrap.*

3.2 Analysis of Pre-Fire Season Precipitation

Trends in observational precipitation levels, from the gridded data products set out in section 2.1, are calculated and compared for the months October to April. Precipitation can directly affect how vegetation grows and develops in a region. Thus, higher precipitation levels, leading to increased vegetation growth, have the potential to develop an abundance of ignition material and sustained fuel for wildfires later in the drier months of the year. Rainfall patterns can determine the type and quantity of vegetation (i.e. grasses) which in turn directly affect the start, spread and containment of wildfires. The timing and duration of the winter rainfall can act as an early indicator of potential wildfire risk. This may be a stronger indication of potential wildfires than the total rainfall over the period but it is significantly more difficult to obtain from observations. As a result, total rainfall for the winter and spring months were chosen for examination as they give an overall indication of potential wildfire hazards.

The months October to April were chosen for investigation as they are the prime growing months for vegetation in the study region. In the winter months leading up to the wildfires, in general, it was dry in Greece and wet in Türkiye. However, across the last number of years there is an overall drying trend in both regions, with this trend being stronger in Türkiye.

First, the precipitation analysis was run for the entire Mediterranean region outlined in section 1.2. The same analysis was then run for the region split in two by 26°E. Therefore, the analysis was run using precipitation observations for three different areas (Table 3.3). They will be referred to as the ‘full’ region, the ‘west’ region (primarily Greece), and the ‘east’ region (primarily Cyprus and Türkiye).

For the precipitation observation in the ‘full’ region, we see a 14% decrease in rainfall totals compared to pre-industrial times. For the ‘west’ region, there is a 5% decrease and for the ‘east’ region, there is a 21% decrease. Therefore, for all regions, the winter months of October to April are

getting drier on average with less rainfall being observed. This would indicate a potential increase in the population of plants which do not need substantial levels of rainfall to sustain growth.

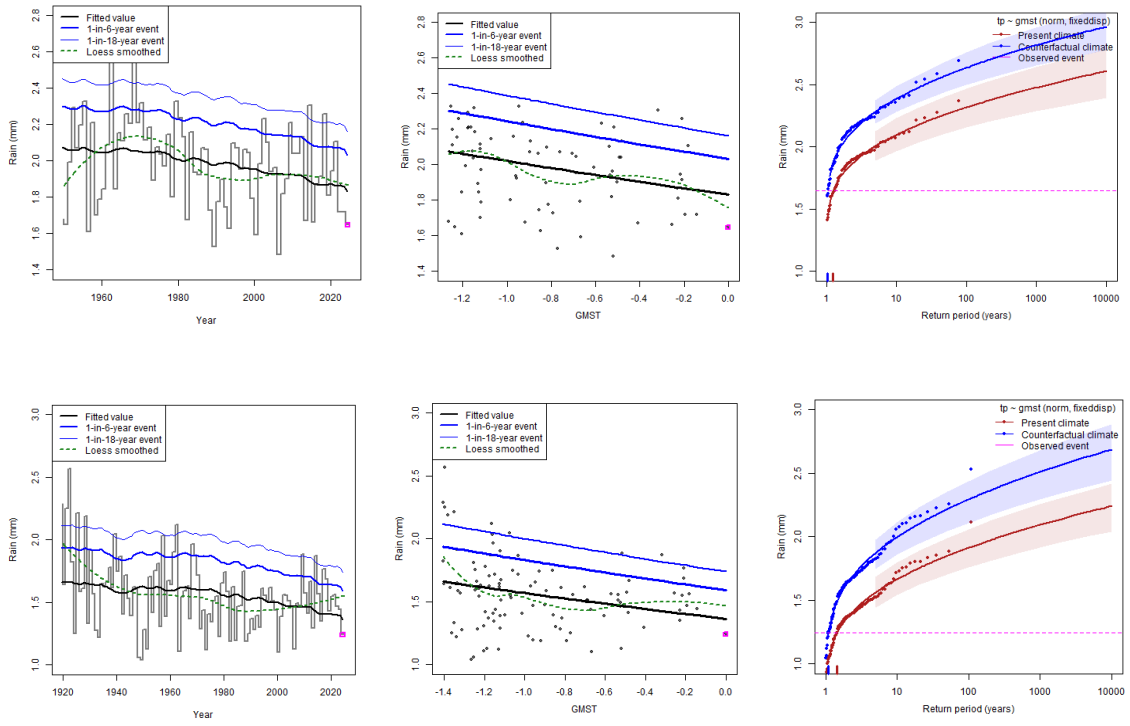

Figure 3.4: *Top row: ERA5 data for the entire Mediterranean region. Bottom row: EOBS data for the entire Mediterranean region. (Left) the trend against time in the 7-month high precipitation event. (Centre) the trend against GMST in the 7-month high precipitation event. (Right) the log-normal shift of the 7-month high precipitation event distribution to GMST, return periods are shown for the 2025 climate (red) and a climate with GMST 1.3°C cooler (blue). The reanalysis data are shown twice: once shifted up to the current climate and once shifted down to the climate of the pre-industrial era. The markers show the data and the lines show the fits and uncertainty from the bootstrap.*

Table 3.2: *Estimated probability ratios and change in intensity for seasonal precipitation over Mediterranean Greece, Türkiye and Cyprus in the ERA5 and EOBS reanalysis datasets with coverage of the event.*

Data set	Precipitation (Oct-Apr)			
	Magnitude (mm)	Return period (95% C.I.)	Probability ratio PR	Change in intensity ΔI [%]
ERA5-Land	-	-	-	-
ERA5	1.65	1.24 (1.08…1.53)	0.836 (0.667…0.962)	-12.9 (-20.8…-4.93)
EOBS	1.24	1.43 (1.19…1.86)	0.761 (0.548…0.947)	-14.6 (-24.0…-3.67)

Table 3.3: *Estimated probability ratios and change in intensity for seasonal precipitation over Mediterranean Greece, Türkiye and Cyprus in the ERA5 and EOBS reanalysis datasets with coverage of the event.*

Data set	Precipitation (Oct-Apr) - West				Precipitation (Oct-Apr) - East			
	Magnitude (mm)	Return period (95% C.I.)	Probability ratio PR	Change in intensity ΔI [%]	Magnitude (mm)	Return period (95% C.I.)	Probability ratio PR	Change in intensity ΔI [%]
ERA5-Land	-	-	-	-	-	-	-	-
ERA5	2.01	1.38	0.78 (0.58…0.96)	-13.6 (-20.4…-3.30)	1.60	1.20	0.86 (0.705…0.971)	-12.8 (-22.0…-4.16)
EOBS	1.69	1.74	1.160 (0.719, 1.861)	3.92 (-7.62…18.1)	1.26	1.47	0.712 (0.502…0.887)	-27.4 (-38.2…-14.3)

Precipitation was also inferred through the drought code which is part of the Fire Weather Index used to calculate DSR. Accounting for drought conditions at the time of and preceding the fires, this was one of the driest years ever recorded. 2025 was found to be one of the driest years on record (1950-present) during the peak wildfire period of June-September. It must, however, be noted that the wildfire period of 2025 is still ongoing and so this plot is not fully up to date.

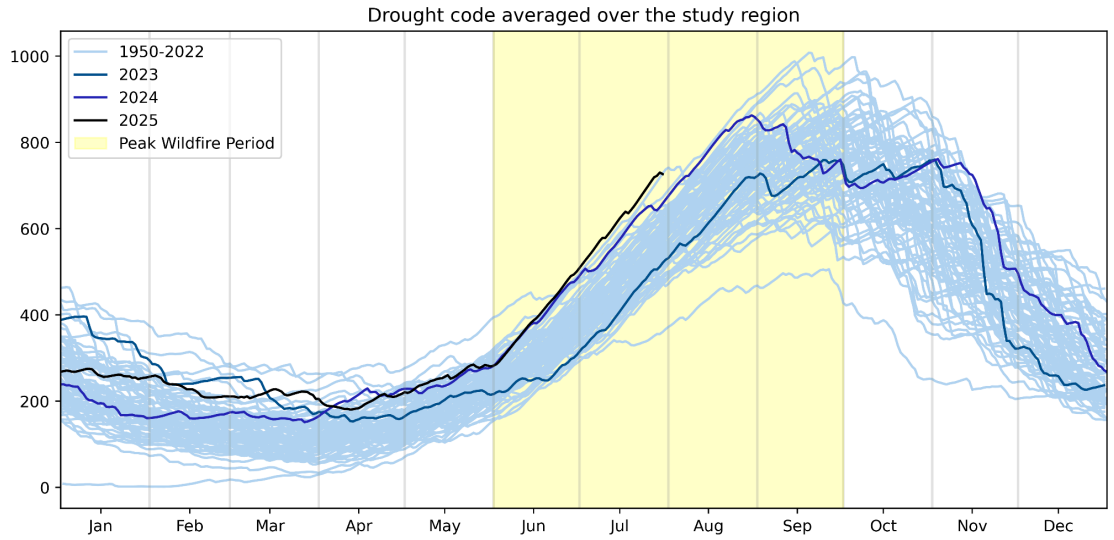

Figure 3.5: *Drought code data from 1950 - 2025. Each line represents a different year. The highlighted period marks the peak wildfire period from June to September. The year of interest, 2025, is represented by the black line.*

4 Model evaluation

In the subsections below we show the results of the model evaluation for each location. The climate models are evaluated against the observations in their ability to capture:

1. **Seasonal cycles**: For this, we qualitatively compare the seasonal cycles based on model outputs against observations-based cycles. We discard the models that exhibit ill-defined peaks in their seasonal cycles. We also discard the model if the rainy season onset/termination varies significantly from the observations.
2. **Spatial patterns**: Models that do not match the observations in terms of the large-scale precipitation patterns are excluded.
3. **Parameters of the fitted statistical models**. We discard the model if the model and observation parameters ranges do not overlap.

The models are labelled as 'good','reasonable', or 'bad' based on their performances in terms of the three criteria discussed above. A model is given an overall rating of 'good' if it is rated 'good' for all three characteristics. If there is at least one 'reasonable', then its overall rating will be 'reasonable' and 'bad' if there is at least one 'bad'. Where the same model was available in multiple different realisations, the first realisation of the model passing the selection criteria was used, to avoid overweighting for that model in the analysis.

4.1 DSR3x

The table below shows the model evaluation results. Models that were rated 'good' and 'reasonable' were used: this resulted in 6 of 13 CORDEX models (including 3 realisations of the same GCM/RCM combination), and 1 of 18 HighResMIP models being used in the analysis.

Table 4.1: *Evaluation results of the climate models considered for attribution analysis of DSR3x. For each model, the threshold for a 1-in-20-year event is shown, along with the best estimates of the Sigma parameters are shown, along with a 95% confidence intervals. Furthermore evaluation of the seasonal cycle and spatial pattern are shown.*

Model / Observations	**Seasonal cycle**	**Spatial pattern**	**Sigma parameter**	**Conclusion**
Observations				
ERA5-Land			0.206 (0.169…0.236)	
Models				
CORDEX				
CNRM-CERFACS-CNRM-CM5_RCA4	bad	bad	0.276 (0.202…0.323)	bad
CNRM-CM5_r1i1p1_ALADIN63	good	good	0.206 (0.161…0.245)	good
CNRM-CM5_r1i1p1_RACMO22E	good	good	0.340 (0.268…0.394)	bad
EC-EARTH_r12i1p1_RACMO22E	reasonable	good	0.184 (0.148…0.214)	reasonable
EC-EARTH_r1i1p1_RACMO22E	reasonable	good	0.198 (0.144…0.230)	reasonable
EC-EARTH_r3i1p1_RACMO22E	reasonable	good	0.203 (0.172…0.226)	reasonable
ICHEC-EC-EARTH_RCA4	bad	bad	0.147 (0.115…0.167)	bad

IPSL-IPSL-CM5A-MR_RCA4	bad	bad	0.174 (0.131…0.220)	bad
MOHC-HadGEM2-ES_RCA4	bad	bad	0.184 (0.148…0.211)	bad
MPI-ESM-LR_r1i1p1_RACMO22E	good	good	0.194 (0.144…0.222)	good
MPI-ESM-LR_r3i1p1_REMO2015	good	reasonable	0.229 (0.175…0.260)	reasonable
MPI-M-MPI-ESM-LR_RCA4	bad	ba	0.189 (0.159…0.218)	bad
NCC-NorESM1-M_RCA4	bad	bad	0.144 (0.115…0.165)	bad
HighResMIP				
CNRM-CM6-1-HR_r1i1p1f2	good	good	0.567 (0.322…0.782)	bad
CNRM-CM6-1_r1i1p1f2	good	good	0.188 (0.152…0.215)	good
EC-Earth3P-HR_r2i1p1f1	bad	good	0.103 (0.0852…0.116)	bad
EC-Earth3P-HR_r3i1p1f1	bad	good	0.31 (0.213…0.355)	bad
EC-Earth3P_r1i1p1f1	bad	good	0.0957 (0.0748…0.111)	bad
EC-Earth3P_r2i1p1f1	bad	good	0.320 (0.25…0.397)	bad
EC-Earth3P_r3i1p1f1	bad	good	0.104 (0.0808…0.121)	bad
HadGEM3-GC31-HM_r1i1p1f1	bad	good	0.126 (0.0919…0.153)	bad
HadGEM3-GC31-HM_r1i2p1f1	bad	good	0.0945 (0.0735…0.106)	bad
HadGEM3-GC31-HM_r1i3p1f1	bad	good	0.100 (0.0841…0.112)	bad
HadGEM3-GC31-LM_r1i14p1f1	bad	good	0.240 (0.193…0.284)	bad
HadGEM3-GC31-LM_r1i15p1f1	bad	good	0.257 (0.208…0.288)	bad
HadGEM3-GC31-LM_r1i1p1f1	bad	good	0.099 (0.0826…0.107)	bad
HadGEM3-GC31-LM_r1i2p1f1	bad	good	0.0949 (0.0798…0.115)	bad
HadGEM3-GC31-LM_r1i3p1f1	bad	good	0.109 (0.082…0.126)	bad
HadGEM3-GC31-MM_r1i1p1f1	bad	good	0.0987 (0.0728…0.114)	bad
HadGEM3-GC31-MM_r1i2p1f1	bad	good	0.0863 (0.0688…0.0981)	bad
HadGEM3-GC31-MM_r1i3p1f1	bad	good	0.307 (0.260…0.351)	bad

4.2 VPD7x

The table below shows the model evaluation results. Models that were rated ‘good’ and ‘reasonable’ were used: this resulted in 4 of 7 CORDEX models, and 1 of 18 HighResMIP models being used in the analysis.

Table 4.2: *Evaluation results of the climate models considered for attribution analysis of VPD7x. For each model, the threshold for a 1-in-10-year event is shown, along with the best estimates of the Sigma parameters are shown, along with a 95% confidence intervals. Furthermore evaluation of the seasonal cycle and spatial pattern are shown.*

Model / Observations	**Seasonal cycle**	**Spatial pattern**	**Sigma parameter**	**Conclusion**
Observations				
ERA5-Land			0.138 (0.115…0.157)	
Models				
CORDEX				
CNRM-CM5_r1i1p1_ALADIN63	good	good	0.140 (0.116…0.160)	good
CNRM-CM5_r1i1p1_RACMO22E	good	good	0.186 (0.153…0.208)	reasonable
EC-EARTH_r12i1p1_RACMO22E	good	good	0.127 (0.096…0.146)	good
EC-EARTH_r1i1p1_RACMO22E	good	good	0.138 (0.115…0.155)	good
EC-EARTH_r3i1p1_RACMO22E	good	good	0.153 (0.131…0.171)	good
MPI-ESM-LR_r1i1p1_RACMO22E	good	good	0.148 (0.111…0.182)	good
MPI-ESM-LR_r3i1p1_REMO2015	good	good	0.150 (0.121…0.168)	good
HighResMIP				
CNRM-CM6-1-HR_r1i1p1f2	good	good	0.097 (0.076…0.114)	reasonable
CNRM-CM6-1_r1i1p1f2	good	good	0.101 (0.077…0.116)	reasonable
EC-Earth3P-HR_r1i1p1f1	good	good	0.083 (0.067…0.093)	bad
EC-Earth3P-HR_r2i1p1f1	good	good	0.087 (0.068…0.098)	bad
EC-Earth3P-HR_r3i1p1f1	good	good	0.070 (0.057…0.080)	bad
EC-Earth3P_r1i1p1f1	good	good	0.084 (0.058…0.099)	bad
EC-Earth3P_r2i1p1f1	good	good	0.083 (0.070…0.092)	bad
EC-Earth3P_r3i1p1f1	good	good	0.085 (0.068…0.095)	bad
HadGEM3-GC31-HM_r1i1p1f1	good	good	0.102 (0.083…0.121)	reasonable
HadGEM3-GC31-HM_r1i2p1f1	good	good	0.076 (0.056…0.088)	bad
HadGEM3-GC31-HM_r1i3p1f1	good	good	0.089 (0.073…0.102)	bad

HadGEM3-GC31-LM_r1i14p1f1	good	good	0.071 (0.056…0.082)	bad
HadGEM3-GC31-LM_r1i15p1f1	good	good	0.094 (0.073…0.103)	bad
HadGEM3-GC31-LM_r1i1p1f1	good	good	0.076 (0.061…0.089)	bad
HadGEM3-GC31-LM_r1i2p1f1	good	good	0.079 (0.064…0.093)	bad
HadGEM3-GC31-LM_r1i3p1f1	good	good	0.074 (0.057…0.089)	bad
HadGEM3-GC31-MM_r1i1p1f1	good	good	0.084 (0.064…0.104)	bad
HadGEM3-GC31-MM_r1i2p1f1	good	good	0.086 (0.069…0.096)	bad
HadGEM3-GC31-MM_r1i3p1f1	good	good	0.087 (0.071…0.100)	bad

5 Multi-method multi-model attribution

This section shows Probability Ratios and change in intensity ΔI between a past climate that is 1.3℃ cooler than now and the current climate for models that passed model evaluation and also includes the values calculated from the fits with observations. For all the models that passed the evaluation test, we show the results between the current climate and a future climate that is 1.3℃ warmer than now.

Table 5.1: *Event magnitude, probability ratio and change in intensity for a 20-year return period for DSR3x for observational datasets and each model that passed the evaluation tests.* ***(a)*** *from pre-industrial climate to the present and* ***(b)*** *from the present to 2.6℃ above pre-industrial climate.*

Model / Observations	Threshold for return period 20 yr	Current warming level [˚C]		Future warming level [2.6˚C]	
		Probability ratio PR [-]	Change in intensity ΔI [%]	Probability ratio PR [-]	Change in intensity ΔI [%]
ERA5-Land	31.2	4.54 (0.572…47.0)	14.4 (-4.18…36.1)		
CNRM-CM5_r1i1p1_ALADIN63	51.9	17.41 (1.87…433)	25.6 (5.64…49.9)	5.98 (1.69…13.0)	20.4 (5.32…33.3)
EC-EARTH_r1i1p1_RACMO22E	61.6	39.7 (6.55…415)	30.83 (15.7…51.5)	7.88 (3.88…13.0)	23.6 (13.6…34.0)
MPI-ESM-LR_r1i1p1_RACMO22E	59.1	5.20 (0.69…84.39)	17.0 (-4.10…43.7)	3.43 (0.67…9.59)	14.5 (-4.27…30.4)
MPI-ESM-LR_r3i1p1_REMO2015	78.3	219 (22.32…4370)	54.6 (32.0…88.5)	11.7 (6.51…16.6)	35.3 (24.2…47.0)
CNRM-CM6-1_r1i1p1f2	82.3	73.31 (4.75…5240)	32.4 (11.8…53.5)	9.30 (3.26…16.8)	24.5 (10.6…34.9)

Table 5.2: *Event magnitude, probability ratio and change in intensity for a 10-year return period for VPD7x for observational datasets and each model that passed the evaluation tests.* ***(a)*** *from pre-industrial climate to the present and* ***(b)*** *from the present to 2.6℃ above pre-industrial climate.*

Model / Observations	Threshold for return period 20 yr	Current warming level [˚C]		Future warming level [2.6˚C]	
		Probability ratio PR [-]	Change in intensity ΔI [%]	Probability ratio PR [-]	Change in intensity ΔI [%]
ERA5-Land	3810 Pa	10.7 (1.76…110)	15.8 (3.15…30.0)		
CNRM-CM5_r1i1p1_ALADIN63	4550 Pa	28.31 (3.02…1580)	20.6 (7.23…38.8)	5.52 (2.33…8.98)	17.1 (6.74…27.9)
CNRM-CM5_r1i1p1_RACMO22E	3150 Pa	2.16 (0.48…16.0)	7.43 (-8.32…23.9)	1.89 (0.398…4.74)	6.92 (-9.07…19.3)
EC-EARTH_r12i1p1_RACMO22E	3900 Pa	13.81 (1.71…613)	18.6 (4.44…36.4)	4.53 (1.59…8.49)	15.7 (4.24…26.7)
EC-EARTH_r1i1p1_RACMO22E	3890 Pa	72.2 (6.24…1080)	26.5 (13.8…37.6)	6.66 (3.35…8.79)	20.9 (12.15…27.3)
EC-EARTH_r3i1p1_RACMO22E	3570 Pa	5.46 (0.84…179)	12.9 (-1.39…32.1)	3.18 (0.82…7.46)	11.4 (-1.41…24.26)
MPI-ESM-LR_r1i1p1_RACMO22E	4390 Pa	26.9 (2.84…513)	26.1 (8.81…46.8)	5.45 (2.25…8.37)	20.7 (8.09…31.9)

MPI-ESM-LR_r3i1p1_REMO2015	5520 Pa	202 (34.6…5130)	32.4 (22.2…46.9)	7.67 (5.78…9.39)	24.5 (18.1…31.9)
CNRM-CM6-1-HR_r1i1p1f2_gr	5030 Pa	34.8 (3.28…832)	15.1 (5.74…23.6)	5.79 (2.45…8.66)	13.1 (5.43…19.1)
CNRM-CM6-1_r1i1p1f2_gr	5020 Pa	4660 (198…996000)	29.5 (18.5…40.9)	9.37 (7.66…9.96)	22.8 (15.6…29.0)
HadGEM3-GC31-HM_r1i1p1f1_gn	6220 Pa	67.9 (5.50…2350)	18.6 (8.82…28.6)	6.59 (3.16…9.14)	15.7 (8.11…22.3)

6 Changes in Circulation

To understand how the atmospheric circulation similar to the 26 July are changing, we use atmospheric flow analogues. These allow us to assess changes in dynamically similar events or shifts in the frequency of circulations (Jézéquel et al., 2018, Thompson et al 2024). Here, we use ERA5 data to assess analogues identified from 500 hPa geopotential height (Z500) since 1950, to detect trends in the frequency of analogue circulations of those that occurred during the fire event.

To identify the most similar events, we compute the Euclidean distance between the Z500 field of the event day and every other day within JJA (1950–2023) over the region bounded by 12° to 40°E, 30° to 48°N. To avoid double-counting persistent events, the identified events must be separated by at least 5 days.

We identify the 26 closest analogues for each day in two periods: an early period (1951–1980) with a weaker climate change signal, and a later period (1994–2023) with a stronger signal. This corresponds to the closest 1% of days in each period. Mean conditions from each analogue set (“composites”) are compared to evaluate differences between periods. Changes in analogue frequency are assessed at thresholds of the upper 5%, 10%, and 20% of days. As differences in internal variability between periods can also affect weather conditions, climate change cannot be inferred solely from analogue comparisons in reanalyses.

On 26 July 2025, a strong ridge dominated the central and eastern Mediterranean, with Z500 values exceeding ~5800 m, indicative of warm, stable conditions in Greece, Turkey and the Balkans (figure 4x). The 1951–1980 composite (b) shows weaker positive anomalies, a less intense ridge, and a sharper north–south gradient. In contrast, the 1994–2023 composite (c) more closely matches the 2025 event, with higher Z500 values and a stronger ridge extending northwards. This shift suggests that ridging patterns similar to the 2025 event have become more pronounced, intensifying heat and promoting northerly wind flow, although the change is not statistically significant. Such differences may reflect a strengthening of these circulation patterns, but attribution to climate change must account for natural variability.

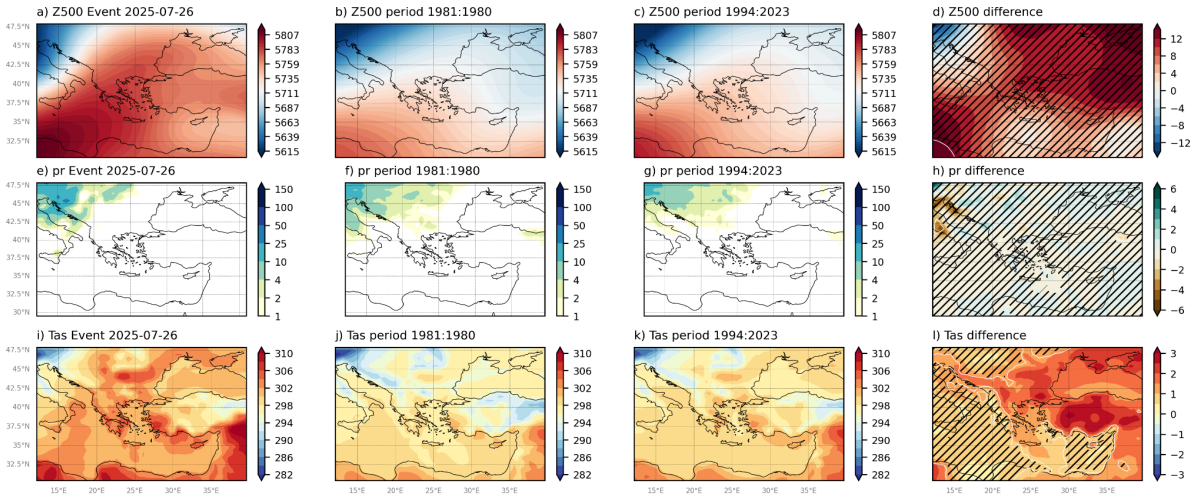

Figure 6.1*: Changes in atmospheric analogues.* ***(a)*** *500hPa geopotential height field (m) for the event, 26 July 2025.* ***(b)*** *Composite of the top 26 analogue days from the past period, 1950-1979.* ***(c)*** *Composite of the top 26 analogue days from the present period, 1994-2023.* ***(d)*** *Difference between the composites of past and present (present minus past).* ***(e-h)*** *as in a-d for the rainfall field (mm).* ***(i-l)*** *as in a-d for the 2m temperature field (°C). Z500 used to identify analogues in all plots. Hashing signifies regions where the signal is not significant based on a two-sided t-test.*

7 Hazard synthesis

DSR3x:

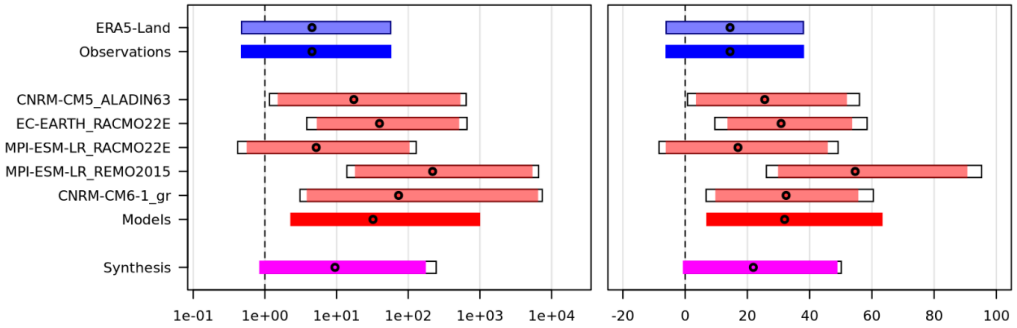

***Figure 7.1**: Synthesis of (left) probability ratio and (right) relative intensity change when comparing DSR3x over the study region with a 1.3℃ cooler climate.*

VPD7x:

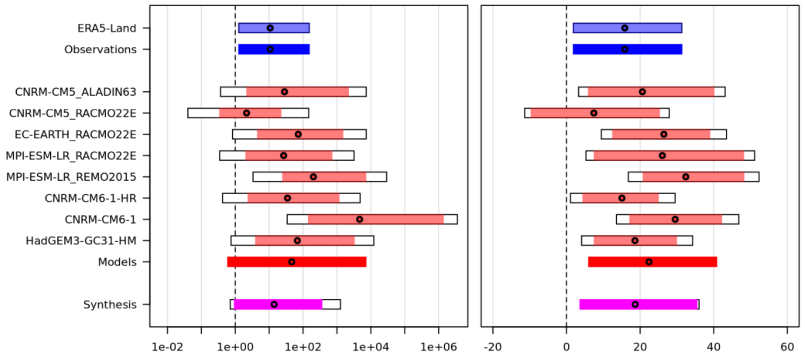

***Figure 7.2**: Synthesis of (left) probability ratio and (right) relative intensity change when comparing VPD7x over the study region with a 1.3℃ cooler climate.*

For the two event definitions described above (sec. 1.2) we evaluate the influence of anthropogenic climate change on these two ways of describing the fire events by calculating the probability ratio as well as the change in intensity using observations and climate models. Models which do not pass the evaluation described above (sec. 4) are excluded from the analysis. The aim is to synthesise results from models that pass the evaluation along with the observations-based products, to give an overarching attribution statement.

Figures 7.1 and 7.2 show the changes in probability and intensity for the observations (blue) and models (red). Before combining them into a synthesised assessment, a term to account for intermodel spread is added (in quadrature) to the natural variability of the models. This is shown in the figures as white boxes around the light red bars. The dark red bar shows the model average, consisting of a weighted mean using the (uncorrelated) uncertainties due to natural variability plus the term representing intermodel spread (i.e., the inverse square of the white bars).

The observation-based product, which in this case is only ERA5-Land as described in section (2), and models are combined into a single result in two ways following Otto et al., (2024). Firstly, we neglect common model uncertainties beyond the intermodel spread that is depicted by the model average, and compute the weighted average of models (dark red bar) and observations (dark blue bar, identical to light blue as only one reanalysis dataset is used): this is indicated by the magenta bar. As, due to common model uncertainties, model uncertainty can be larger than the intermodel spread, secondly, we also show the more conservative estimate of an unweighted, direct average of observations (dark blue bar) and models (dark red bar) contributing 50% each, indicated by the white box around the magenta bar in the synthesis figures.

The results are shown in tables 5.1 and 5.2. As the models generally agree well with each other and also with the reanalysis assessment the unweighted and weighted synthesis are very similar as indicated by the small white bars, we thus provide the weighted synthesis estimates in table 7.1.
Again, as models and observations show very similar results, that are in most cases statistically significant and well bounded (the 95% confidence interval is comparably narrow) we communicate the best estimates of the synthesised results as the overarching results: An increase in intensity of about 18% for VPD7x and also about 22% for DSR3x, and an increase in likelihood of a factor of about 13 for VPD7x and about 10 for DSR3x. These synthesised results are statistically significant - the 95% confidence intervals do not encompass the possibility of no change.

Since only five out of 31 models passed the evaluation tests for DSR3x, which is a relatively small subset, we also inspect the results using all climate models for DSR3x to see whether these models show totally different behaviour in trends. The general picture is however consistent with the results where only 'good' models are used in the synthesis.

When performing the same analysis but for a 1.3°C warmer future from today, representing an overall global warming of 2.6°C, we find very similar results to the synthesised for the past, with again an additional increase in intensity of another 20% (18% for VPD7x and 25% for DSR3x), corroborating that the changes seen in the past are indeed due to anthropogenic climate change. As the results imply probabilities will become close to one (the event happens on average every year) we do not communicate changes in probability for the future climate.

We communicate these synthesised results alongside the observed decrease in winter rainfall totals, described in section 3.2, as well as the circulation assessment (sec. 6) that suggests these types of high-pressure systems have become more intense, leading to more intense heat and stronger northerly winds. Thus, all our analysis, the fire weather indices as well as the preceding rainfall and the circulation analogues point in the same direction, a strong increase in fire weather risk due to human induced climate change.

Data		VPD7x		DSR3x	
		Probability ratio (95% CI)	**Intensity change (%) (95% CI)**	**Probability ratio (95% CI)**	**Intensity change (%) (95% CI)**
Observations	**Past-Present**	**10.7 (1.76 - 110)**	**15.8 (3.15 - 30.0)**	4.54 (0.572 - 47.0)	14.4 (-4.18 - 36.1)
Models		32.4 (0.74 - 3110)	**21.5 (7.61 - 38.1)**	**32.3 (2.8 - 813)**	**32.0 (8.91 - 61.3)**
Synthesis		**13.3 (1.3 - 246)**	**18.4 (4.94 - 33.7)**	**9.51 (1.03 - 142)**	**21.9 (1.41 - 46.8)**
Models only	**Present-Future**	**6.24 (2.37 - 12.9)**	**18.0 (7.12 - 28.1)**	**8.52 (3.10 - 17.3)**	**24.8 (9.43 - 39.0)**

Table 7.1: *Summary of results for both event definitions, VPD7x and DSR3x, presented in Figs 7.1 and 7.2: changes due to GMST include past-present changes and present-future changes. Statistically significant changes are also highlighted in* ***bold*** *font.*

8 Vulnerability and exposure

The Mediterranean region, including the countries of Türkiye, Greece, and Cyprus, is inherently susceptible to wildfires due to the convergence of climatic, ecological, and socio-economic factors. Its hot, dry summers, often with temperatures exceeding 30℃, create highly combustible landscapes; a risk further intensified by strong winds that accelerate fire spread.

In the summer of 2025, Greece, Cyprus, and Türkiye faced some of the most severe wildfires in recent memory, underscoring the escalating risks posed by extreme heat, prolonged drought conditions, and strong winds. In Greece, temperatures exceeded 45℃ and large-scale fires ignited that destroyed tens of thousands of acres, forced thousands of evacuations, and severely disrupted tourism and agriculture (IFRC, 2025; Le Monde, 2025; Giannopoulos, 2025). Cyprus experienced parallel devastation, with fires north of Limassol burning nearly 1% of the island, killing two people, damaging over 70 homes, causing power outages, and devastating olive groves and vineyards (Euronews, 2025; Reuters, 2025; Al Jazeera, 2025a). In Cyprus the fires were exceptional due to the area burned which was an order of magnitude higher than recorded in the last 20 years of records (EFFIS, 2025). Türkiye has faced one of the most devastating wildfire seasons in its history. By mid-July, more than 600 fires had been recorded; at least 17 people lost their lives (the majority consisting of forestry workers and AKUT rescue volunteers), over 50,000 people and more than 8,000 livestock were evacuated. Major traffic routes were disrupted across several provinces, including İzmir, Bursa, Manisa, Bilecik, Hatay, Çanakkale, and Eskişehir, with more than 1,000 buildings and barns destroyed (General Directorate of Forestry, 2025; Bianet, 2025a; Bianet, 2025b; ECHO Flash, 2025; Reuters, 2025; Al Jazeera, 2025b; Daily Sabah, 2025a; Daily Sabah, 2025b; BirGün, 2025; CSB, 2025; TRT Global, 2025, Euro News, 2025). Collectively, these disasters highlight how climate-driven extremes are intensifying wildfire activity while amplifying cascading impacts across housing, health, infrastructure, agriculture, and tourism.

While these wildfires are quite severe, they are not, at the time of writing, at the level of catastrophic 2021 fire season in which 170K and 125K Hectares were burned in Turkiye and Greece, respectively, requiring widespread evacuations, and leading to large scale blackouts, infrastructure loss, and impacts to tourism (JRC, 2022)

All three countries rank very high on the Human Development Index (Cyprus 0.907; Greece 0.893; Türkiye 0.855) (UNDP, 2022), yet they face differing levels and patterns of wildfire risk.

8.1 Exposure and land management

Wildfire exposure and land use and land cover management across the Mediterranean are shaped by fire-prone vegetation, changing land-use practices, and expanding settlement in the wildland-urban interface (WUI), the transition zone between unoccupied vegetated land and human development.

In Türkiye, forests cover about 30% of its land area, dominated by highly flammable Turkish pine (The Forests Associations of Türkiye, 2024; Iban, 2022). Fires are driven by heatwaves, drought, and human activity, with nearly 89% of ignitions directly or indirectly caused by people (Ekberzade, 2025). Negligence, such as discarded cigarettes, stubble burning, and powerline faults, accounts for a

large share of outbreaks (Sari, 2023). Agricultural residue burning has degraded soils and water quality, further compounding vulnerability (Yakuboglu 2022). Exposure is aggravated during May through November, when fire season coincides with peak tourism (Sonmez, 2025).

In Greece, about 50% of land is forested, two-thirds of which is state-managed (Xepapadeas, 2024). According to the 2022 analysis of the Hellenic Land Registry (2022), forested areas have increased by about 445,620 hectares in the last 80 years, from 6,967,914 hectares in 1945 to 7,413,549 in 2022. This increase is due to various factors, such as rural abandonment, decline in extensive livestock farming (forest cover particularly expanded in mountainous areas that were once used for farming or grazing), special protective legislation, as well as reforestation and forest management measures that helped restore old forests. (Votaniki, n.d.; General Directorate of Forests and Forest Environment, n.d.). Conversely, in coastal areas the increase was smaller due to urbanization and tourism development. As such, the country has an exceptionally wide range of forest ecosystems, stemming from its rich biodiversity and complex environmental structure. The presence of multiple climate types - ranging from typical Mediterranean to continental - combined with the country's mountainous terrain and numerous islands, significantly contributed to the formation of diverse micro-environmental conditions. In addition, the geological diversity and variety of soil types create ideal conditions for the development of various forest types and ecosystems, giving them a polymorphic and dynamic character (General Directorate of Forests and Forest Environment, n.d.). Vegetation flammability and hot, windy summers create high fire risk, especially in WUIs. Since the 1970s, rural depopulation and gradual abandonment of agricultural plots have altered land management, contributing to fuel build-up and changing fire behavior (Sparks et al., 2024). At the same time, expansion of settlements into fire-prone areas has added ignition sources and increased exposure, leaving both rural and peri-urban communities highly vulnerable (Xanthopoulos, 2015).

Cyprus has approximately 25% forest cover, comprising a mix of state-owned and private forests interspersed with maquis (dense Mediterranean shrubland), garrigue (open, low scrub on rocky soils), and agricultural land (Fernandez-Anez et al., 2021). The abandonment of traditional practices - such as grazing, cultivation, and controlled burns - has led to significant accumulation of flammable biomass. This mirrors trends across the Mediterranean rather than indicating a uniquely Cypriot challenge (Ministry of Agriculture, Natural Resources and Environment, 2010). Human negligence continues to drive fire ignitions, particularly in rural wildland-urban interface areas where isolated homes, farms, and tourist resorts are increasingly vulnerable (Fernandez-Anez et al., 2021).

While Türkiye and Greece face similar challenges with large-scale fires that can span multiple provinces, large summer tourist populations and fire-conducive environments, the wildland urban interface (WUI) in Turkiye is mainly in coastal tourist areas and inland forest villages, whereas in Greece the risk is particularly high in dense island settlements and in the Attica suburbs presenting different firefighting and evacuation challenges (Mitsopoulos, 2020; Aksoy et al., 2023; Guney et al, 2019). Cyprus faces concentrated risks due to its small size and reliance on aerial support for large fires (Pandey et al., 2024).

Wildfires in Greece, Cyprus, and Türkiye disproportionately affect livelihoods tied to rural and forested landscapes. In Greece, agriculture and farming (particularly olive groves, vineyards, orchards, and grazing lands) suffer repeated losses, in addition to beekeeping, animal husbandry, and

ecotourism, which depend on intact ecosystems (Hess, 2025; Groom, 2023). In Cyprus, vineyard owners and small farmers are heavily impacted, with damage extending to livestock, infrastructure, and local businesses, reducing both agricultural and non-agricultural employment opportunities (Al Jazeera, 2025; Karagiorgas, 2025; Kourtoglou, 2025). In Türkiye, wildfires disrupt forest-based livelihoods, including olive farming, goat herding, bay leaf cultivation, and the collection of forest products (Kuran, 2023; Cookman, 2021). Beekeeping, especially pine honey production in Mugla Province, faces long-term decline due to the destruction of forest habitats (Kuran, 2023).

These exposure patterns highlight how human pressures and land governance converge, making strategic frameworks for regulation, planning, and risk reduction central to addressing wildfire dynamics.

8.2 Legislation, Policy, and Prevention

In Turkiye, the government has adopted robust policies on preventing wildfires. In a review of Turkish forestry legislation, it was found that collectively it follows the FAO's guidance with about 78.1% accuracy, and includes important anchors such as the constitutional guarantee to reforest burned forested land. (Elvan, 2021). The country's forestry legislation focuses on policies preventing the spread of wildfires and penalties for intentionally setting forest fires are severe (minimum 10 years imprisonment) (Elvan, 2021). During high-risk periods, public entry into forested areas is restricted in order to reduce accidental ignitions (AzerNews, 2025). This year, Turkiye promoted a "forest is mine" campaign to increase public awareness of wildfires risks and guidelines for prevention (TurkiyeToday, 2025)

Cyprus has developed a comprehensive legal and institutional framework to manage wildfire risk, anchored in the Forest Law of 2012 (Article 32), which regulates burning activities, prohibits open fires within and around forest areas, and mandates permits and rapid response mechanisms (Ministry of Agriculture, Natural Resources and Environment, 2010; n.d.). Older legislation, such as the 1946 Forest (Protection against Incendiarism) Law, further empowers authorities to act swiftly against suspected offenders. In recent years, penalties have been significantly increased, with forest fire offences carrying up to 12 years' imprisonment or fines of €100,000 (Nicolau, 2024). Implementation is led by the Department of Forests through coordinated prevention, detection, and suppression systems supported by aerial firefighting, operational planning, and collaboration with EU mechanisms for cross-border emergencies (Department of Forests, n.d.-a; n.d.-b). While human activity remains a predominant cause of wildfire ignition - consistent with patterns across the region - this analysis emphasizes that such risks are shared throughout the Mediterranean, rather than implying uniquely Cypriot culpability.

In Greece, the Ministry of Climate Crisis and Civil Protection oversees wildfire management, coordinating prevention, response, and interagency collaboration (Wardropper, Sparks & Hovardas, 2025). Since its establishment in 2021, the ministry has expanded firefighting capacity to more than 18,000 permanent and seasonal staff, supported by a fleet of 3,700 vehicles, 80 drone bases equipped with thermal imaging for early detection, and 20 specialized Forest Commando Units (EMODE) totaling over 1,500 personnel (Hoey, 2025). The Fire Service's fleet also includes 10 firefighting vessels stationed at six Coast Guard Fire Stations, strengthening maritime firefighting, navigation

safety, and rescue capacity (Ministry of Climate Crisis and Civil Protection, 2024). Legislation requires landowners to clear flammable vegetation by April each year, with fines for violations, while a 2024 law introduced harsher penalties for arson (Wardropper, Sparks & Hovardas, 2025). In addition, certain bodies, such as railway services, are obliged to avoid fire instigation, an important fire risk mitigation action (Oikodynamics, n.d.). These measures are embedded in a broader legal framework, including Law 998/1979 on forest protection and suppression duties, and Law 4824/2021, which prohibits wildfire-triggering activities nationwide (Ministry of Environment and Energy, 2022). According to Eurostat, Greece ranks third in Europe in firefighters per capita, reflecting its high level of institutional preparedness. Substantial investments have also been directed toward prevention: over €600 million under the AntiNero programs for forest cleaning and firebreaks, €210 million allocated in 2025 to upgrade 24,000 hectares of forest land, and €40 million provided to municipalities for civil protection (Ministry of Climate Crisis and Civil Protection, 2025).

While regulatory and planning frameworks establish the foundations for risk mitigation, their effectiveness ultimately depends on timely surveillance, coordinated operational capacity, and the ability to constrain fire spread.

8.3 Detection, Response, and Containment

Across the Mediterranean, wildfire management increasingly hinges on rapid detection, coordinated response, and robust suppression capabilities.

By 2025, Türkiye's wildfire response infrastructure had significantly expanded, encompassing an aerial fleet of 27 planes and 105 helicopters, thousands of fire ponds, AI-based detection systems, and numerous watch towers (T.C. Iletisim Baskanligi, 2025). The General Directorate of Forestry (DGF), which controls 99% of forest lands, coordinated this centrally organized response with 25,000 trained personnel and 132,000 volunteers. In addition, nearly 39,000 trained community volunteers were mobilized nationwide to support frontline operations (Daily Sabah, 2025). The Turkish Red Crescent (TRC) played a critical humanitarian response role, participating in 156 wildfire operations by 20 August, deploying 623 staff and 1,221 volunteers, and distributing over 3 million relief items to people affected. In 2024, Türkiye also launched a $400 million "Climate Resilient Forests Project" with the World Bank to strengthen long-term resilience through sustainable forest management, restoration, and community preparedness (World Bank, 2024). These combined measures underscore Türkiye's multi-layered approach: enhancing immediate response capacity, delivering humanitarian relief, and investing in long-term resilience against escalating wildfire risks driven by climate change.

In Greece, since the 1990s, the Hellenic Fire Service, part of the Ministry of Climate Crisis and Civil Protection, has managed response to wildfires, and has had a long history of wildfires through which it has evolved its fire management approach. In July and August of 2025, Greece mounted a large-scale response that combined national resources - about 4,800 firefighters, 360 vehicles, and 62 aircraft - with extensive international support through the EU Civil Protection Mechanism, which mobilized firefighting planes, helicopters, and ground teams from across Europe to assist evacuations, suppression, and monitoring under extreme heat and wind conditions (IFRC, 2025; ECHO, 2025a; ECHO, 2025b; Hoey, 2025). There were evacuations and a major effort was made through warning messages from the emergency number 112 to inform citizens and provide protection instruction. At

the same time, the Ministry of Climate Crisis and Civil Protection and supporting actors, due to Greece's ongoing tourist season, made every effort to better manage incidents of fires in tourist areas. Greece's geomorphological diversity presents a challenge, significantly increasing the difficulty of firefighting. Numerous mountain terrains, steep slopes, and distinct microclimatic zones create complex and hard-to-reach areas that hinder the access of firefighting forces. Moreover, varying slopes and changing winds in mountainous regions dynamically affect fire spread, making prediction and control particularly complex. In the country, suppression of wildfires involves the Fire Service, Air Force, army and local volunteer firefighters (Wardropper et al., 2025). Greece integrates over 10,000 certified volunteers into wildfire response, who bring the advantage of knowing local roads and being able to quickly mobilize (Wardropper et al., 2025; Hoey, 2025). Additionally, the Hellenic Red Cross (HRC), through its staff and volunteers, supported the state and citizens across Greece through the readiness of all its Regional Branches. Guided by its president, Dr. Antonios Avgerinos, the organization implements awareness and education programs on emergency management for citizens as part of its Climate Change Strategy. It also maintains logistical resources, including water, medical supplies, and equipment, to ensure readiness. During emergencies, the HRC activates its operations center to coordinate the work of health services, rescuers and lifeguards, social welfare teams, and search units in affected areas. Its involvement continues into the recovery phase, where psychologists and social workers provide psychosocial support and assess community needs in fire-impacted regions. Ongoing national initiatives include completing national forest maps (Cadestre) and modernizing civil protection systems through EU-backed programs such as AIGIS (Hoey, 2025).

In Cyprus, wildfire suppression is led by the Department of Forests in coordination with the Fire Brigade, Civil Protection, and local authorities, supported by aerial assets and volunteers. In July 2025, intense wildfires in the Limassol District - spurred by a heatwave with temperatures peaking over 44C - destroyed approximately 125 km2 of land, causing at least two fatalities, injuring at least 16 people, and prompting evacuations across 16 communities. Cyprus showcased important advances in wildfire detection and management. The Cyprus Institute piloted an innovative system using geostationary satellite data and supercomputing, capable of detecting smoke within 1 km2 and fire outbreak within 2 km2 and providing near-real time alerts to the Forestry Department (DoF) and Fire Service (BGNES, 2025; Gregoriades, 2025). The parallel Early Warning System (EWS) for public alerts, mandated under EU law, is still undergoing a phased rollout, with full implementation expected in 2026 (Hoey, 2025). Firefighting involved over 250 personnel, supported by 75 fire engines, 14 aircraft, and international aid from Jordan, Spain, Israel, Lebanon, and the United Kingdom. The island's limited domestic aerial firefighting capacity means disproportionate reliance on EU and international emergency support. Post-crisis assessments have noted delays in requesting assistance and gaps in alert dissemination. Investigations are underway to evaluate response delays and the rollout of the EWS, which is not expected to the fully operational before 2026 (Hoey, 2025). The Cyprus Red Cross Society (CRCS) also played a pivotal humanitarian role in supporting affected communities. Mobilizing its nationwide volunteer network, the CRCS provided immediate relief including water, food, first aid, and psychological support to evacuees and frontline responders. The organization assisted with shelter management for displaced families, coordinated donations, and ensured that vulnerable groups such as the elderly, children, and persons with disabilities received targeted assistance. In parallel, CRCS teams worked closely with the Department of Forests, Civil Defense, and local authorities to strengthen evacuation logistics and communication with affected villages. Beyond the emergency phase, the CRCS has remained engaged in longer-term recovery, offering psychosocial support and aid to households whose homes and livelihoods were destroyed.

Volunteers across Cyprus also rapidly mobilized to aid both evacuation and relief operations. Local groups and citizens opened their homes to displaced families, implemented ad hoc shelters, and supported logistics and firefighting efforts (Mantzipa, 2025). Operations like "Firefighters Of The World - Cyprus" are actively training volunteers, via programs supported by the Fire Department, Forestry Department, and Civil Defense, to assist in forest fire and search-and-rescue operations (FoTW-Cyprus, n.d.). Rooted in local knowledge and rapid mobilization, these efforts add a critical bottom-up layer of resilience, complementing official response mechanisms.

The European Union Civil Protection Mechanism (UCPM) has become a critical instrument for addressing wildfire emergencies that surpass national capacities. Through this mechanism, resources and personnel can be rapidly mobilized across borders both reactively and as part of seasonal preparedness. For the 2025 fire season, nearly 650 firefighters from 14 European countries were pre-positioned in high-risk areas including Greece, which also received four medium amphibious aircraft to reinforce aerial firefighting capacity (Hoey, 2025). Such deployment enhances collective readiness and ensures timely rollout of assistance. The mechanism has been activated 16 times for wildfires in 2025, including by Greece, Spain, Bulgaria, Montenegro and Albania over a seven-day period, which is already equal to the number of wildfire activations in 2024 (European Commission, 2025),

8.4 Insurance

In Türkiye, wildfire losses are only partially insured under voluntary property schemes, but reforms are underway to expand coverage (Bahar, 2024). Policies feature fixed premiums and limits, though wildfire-specific caps are not clearly disclosed, and an "Immediate Needs Coverage" component offers rapid financial relief to affected households (Bahar, 2024). Complementing insurance reforms, the government and World Bank launched the $400 million Türkiye Climate Resilient Forests Project in 2024, targeting wildfire management and resilience across 14 high-risk provinces (World Bank, 2024).

In 2025, wildfire insurance for Greek residents and property owners is largely voluntary. Property insurance covering wildfire damage is available, but not legally mandated, leaving many households financially exposed; losses have already cost insurers tens of hundreds of millions of dollars (Commercial Risk, 2024; Morning Star, 2025). In March 2025, only 18.2% of residences were insured (Athens Times, 2025). Vehicle insurance, which is mandatory, typically includes fire damage, while state social insurance provides health and life coverage but not compensation for property losses (Loko, 2025). A new 2025 law, Law 5116/2024, now requires large companies to secure "natural disaster" coverage, including wildfire, suggesting growing recognition of escalating risk (Climate Change Laws of the World, 2024).

Cyprus' wildfire-related insurance in 2025 is also grounded mainly in voluntary coverage, and property insurance remains the primary instrument for protecting homes and businesses in fire-prone areas (Kalmuk, 2025). Comprehensive vehicle insurance often includes fire damage, though coverage for extreme weather is not legally required. Similar to Greece, state social insurance provides health and life protection, but does not extend to property losses (Kalmuk, 2025).

The growing intensity and frequency of fire weather conditions raise concerns about the affordability and availability of coverage. In Greece, for example, large parts of the country have already been classified as "red zones" by insurers, limiting access to affordable property insurance (Athens Times, 2025). This trend reflects broader challenges identified by OECD (2023), with rising physical climate risks increasing the likelihood that high-exposure areas could become "uninsurable." Such trends contribute to a widening protection gap, as voluntary insurance schemes remain limited in uptake and insurers recalibrate risk models, premiums, and exclusions. Over time, this risks reducing financial resilience for households and businesses in fire-prone regions across the three countries.

8.5 V&E Conclusions

Wildfires are part of a yearly cycle of risks that people in the Mediterranean region have found ways to manage and live alongside. Türkiye's vast size, extensive forest cover, and large rural population create widespread exposure and challenges for suppression across diverse terrains. Greece combines mountainous landscapes with high seasonal tourist influxes across thousands of islands, straining evacuation and emergency systems. Cyprus, by contrast, faces more concentrated risks with a small geography and heavy economic reliance on agriculture and tourism, which intensify the consequences of fire. While each of these countries faces significant and increasing risks, they have also strengthened their capacities in recent years, especially following the catastrophic 2021 wildfire season. Since then, Greece and Turkiye have particularly leveraged AI and drones to improve the quick detection of wildfires, so that response can happen quicker, and increased firefighting resources. In Cyprus, there have been efforts to adopt integrated fire management plans, improve community evacuation during fires, and speed adoption of an early warning system, while support from other countries has bridged capacity gaps. As climate change worsens fire weather, there are opportunities to improve preparedness even further. This can include further educating the public about wildfire risks and fire safety behaviors, increasing investment in proactive wildfire mitigation and management, and integrating Indigenous, traditional, and contemporary fire management practices into policy (UNEP, 2022).

Data availability

All time series used in the attribution analysis are available via the Climate Explorer.

References

All references are given as hyperlinks in the text.